Journal of Nuclear Medicine, published on July 8, 2021 as doi:10.2967/jnumed.120.256982

PET tracing of biodistribution for orally administered ^{64}Cu-labeled polystyrene in mice

Authors: Changkeun Im[1,2,†], Hyeongi Kim[1,†], Javeria Zaheer[1,2], Jung Young Kim[1], Yong-Jin Lee[1], Choong Mo Kang[1,2,*], and Jin Su Kim[1,2,*]

Affiliations:

[1]Division of Applied RI, Korea Institute of Radiological and Medical Sciences (KIRAMS), 75 Nowon-ro, Nowon-gu, Seoul 01812, Korea.

[2]Radiological and Medico-Oncological Sciences, University of Science and Technology (UST), 75 Nowon-ro, Nowon-gu, Seoul 01812, Korea.

First authors:

Changkeun Im

Email: ckleader@kirams.re.kr

Hyeongi Kim

Email: erwin.hyeongi@gmail.com

*Correspondence to:

Choong Mo Kang

Tel: +82-2-970-1628

Fax: +82-2-970-1986

Email: ck190@kirams.re.kr

Jin Su Kim

Tel: +82-2-970-1661

Email: kjs@kirams.re.kr

† These authors contributed equally to this work.

Author contributions: Conceptualization, J. S. K and C. M. K.; writing-original draft preparation, C.I, H. K, and C. M. K.; writing-review and editing, J. S. K and C. M. K.; Review, J. Y. K; Funding acquisition, J. S. K and Y.-J.L.; Proofreading-J.S.K and C. M. K.; Experimental work, C.I and J. Z; Data analysis, C.I and H. K..

Competing interests: The authors declare no conflicts of interest. The funders had no role in the design of the study, in the collection, analyses, or interpretation of data, in the writing of the manuscript, or in the decision to publish the results.

Keywords: Microplastic, Polystyrene, Copper-64, [^{64}Cu]Cu-labeled polystyrene, Positron emission tomography

ABSTRACT

Purpose: Plastics are used commonly in the world because of its convenience and cost-effectiveness. Microplastics, an environmental threat and human health risk, are widely detected in food, and consequently ingested. However degraded plastics are found everywhere, which cause environmental threat and human health risk. Therefore, real-time monitoring of orally administered microplastics is tremendously important to trace them in the body.

Methods: In this study, to visualize their absorption path, we labeled polystyrene with [^{64}Cu]Cu-DOTA. We prepared radiolabeled polystyrene with ^{64}Cu after, [^{64}Cu]Cu-DOTA-polystyrene was then orally administered to mice and evaluate its transit and absorption in mice using PET imaging. The absorption path and distribution of [^{64}Cu]Cu-DOTA-polystyrene were determined using positron emission tomography (PET) over 48 h. *Ex vivo* tissue-radio thin-layer chromatography (*Ex vivo*-radioTLC) was used to demonstrate the existence of [^{64}Cu]Cu-DOTA-polystyrene in tissue.

Results: PET images demonstrated that [^{64}Cu]Cu-DOTA-polystyrene began to transit to the intestine within 1 h. [^{64}Cu]Cu-DOTA-polystyrene accumulation in the liver was also observed. Biodistribution of [^{64}Cu]Cu-DOTA-polystyrene confirmed the observed distribution of [^{64}Cu]Cu-DOTA-polystyrene from PET images. *Ex vivo*-radioTLC was used to demonstrate that the detected gamma rays originated from [^{64}Cu]Cu-DOTA-polystyrene.

Conclusion: This study provided evidence of microplastic accumulation and existence in tissue by using PET imaging, and cross confirmed by *ex vivo*-radioTLC. The information provided may be used as the basis for future studies on the toxicity of microplastics.

INTRODUCTION

Microplastics (MPs) with diameters less than 5 mm are recognized as a new environmental threat and human health risk *(1)*. MPs have been observed to accumulate in many different marine animals, including marine fish (*2-5*), Copepod (*6,7*), Mussel (*8-10*), European flat oysters (*11*) and other marine animals (*12-14*). Fiber-type MPs were found in mussels purchased at markets in Belgium (*15*). Considering that MPs are widely detected in food, we can assume that MPs are ingested along with the contaminated food. Therefore, it is highly likely that human consumption of MPs is widespread. To understand the full significance of MP ingestion, the absorption path for MPs ingested with foods needs to be visualized.

Positron emission tomography (PET) imaging is a powerful tool for observing absorption, distribution, metabolism, and excretion (*16*). PET can also be used to visualize the *in vivo* distribution of toxic substances labeled with radioactive isotopes, including diesel exhaust (*17*), and inhaled aerosol particles composed of toxic household disinfectants (*18*). Fig. 1 shows a schematic of this study. We first identified the absorption path and distribution of MPs using PET. MP polystyrene was labeled with Copper-64 ([^{64}Cu]Cu, to yield [^{64}Cu]Cu-DOTA-polystyrene), and then orally administered to mice. In a separate experiment, ^{64}Cu was orally administered as a control to assess the effects of the harsh stomach conditions on de-chelated ^{64}Cu. PET was performed to monitor the absorption and distribution of [^{64}Cu]Cu-DOTA-polystyrene and/or ^{64}Cu over 48 h. The *ex vivo* biodistributions of [^{64}Cu]Cu-DOTA-polystyrene and/or ^{64}Cu were measured. *Ex vivo* tissue-radio thin-layer chromatography (*Ex vivo*-radioTLC) was performed to identify whether gamma rays emitted from the tissue originated from [^{64}Cu]Cu-DOTA-polystyrene or ^{64}Cu.

MATERIALS AND METHODS

Synthesis and Radiolabeling

2.5 mg of amino-polystyrene (0.2–0.3 μm, Spherotech, Lake Forest, IL, USA) was added to 300 μL of 0.1 M sodium carbonate buffer (pH 9.0). 260 μg (471.70 nmol) of S-2-(4-isothiocyanatobenzyl)-1,4,7,10-tetraazacyclododecane tetraacetic acid (*p*-SCN-Bn-DOTA) in 50 μL of deionized water was added and mixture (pH 9.0) was shaken at 1000 rpm and 25 ℃ for 20 h. Unconjugated *p*-SCN-Bn-DOTA was removed using an Amicon centrifugal filter (30 kDa cut-off, Millipore, Billerica, MA, USA). DOTA conjugation was confirmed using fourier-transform infrared (FT-IR) spectroscopy (Nicolet iS5, Thermo Fisher Scientific, Waltham, MA, USA) and the resulting spectra were analyzed using an Omnic software from Nicolet Instrument Corp. (Madison, WI, USA). To determine moles of DOTA per milligram of plastic, 50 μL of filtrate was analyzed by high performance liquid chromatography (HPLC, Waters, Milford, MA, USA). Quantity of DOTA in the filtrate was calculated from a standard curve (prepared from an analysis of known concentrations of DOTA). The conjugated moles of DOTA to polystyrene were then calculated by subtracting the moles of DOTA in the filtrate from the total moles of DOTA for the reaction. Physicochemical characterization of DOTA-polystyrene was performed using FE-SEM, and DLS. Concentrated DOTA-polystyrene was subsequently buffer-exchanged to isotonic buffered saline (IBS) for subsequent radiolabeling. The final concentration before radiolabeling was 2.5 mg/100 μL concentration.

Cyclotron-produced [^{64}Cu]$CuCl_2$ was dried and re-dissolved in 0.01 N HCl (final concentration, 9.25 MBq/μL). 155.4 MBq of [^{64}Cu]$CuCl_2$ was added to 80 μL of 0.1 M NaOAc buffer (pH 5) in a 1.5 mL-tube. DOTA-polystyrene (2 mg in 80 μL) was added and mixture was shaken in a Thermomixer C (Eppendorf AG, Hamburg, Germany) at 40 ℃ and 1000 rpm for 30 min. ^{64}Cu-labeled DOTA-polystyrene was purified using an Amicon centrifugal filter at 25℃, 3000 rpm, for 30 min. By repeating this procedure, reaction buffer was exchanged to 1× PBS for further studies.

In vitro stability study

[^{64}Cu]Cu-DOTA-polystyrene in PBS (1.85 MBq/30 μL) was diluted in 270 μL of PBS, hydrochloric acid-potassium chloride buffer (pH 2), human serum, or mouse serum. Each sample

was incubated at 25℃ (buffer) and 37℃ (serum) for 48 h. %Stability was analyzed using instant TLC (0.1 M citric acid in water as a mobile phase).

PET/CT imaging

All animal experiments were performed under the institutional guidelines of the Korea Institute of Radiology and Medical Sciences (KIRAMS). BALB/c nude mice (n=5–7, 5 weeks old, Shizuoka Laboratory Center, Japan) was used.

PET/CT images were acquired with a Siemens Inveon PET scanner (Siemens Medical Solutions, Germany). [^{64}Cu]$CuCl_2$ (4.81 MBq/100 μL) or [^{64}Cu]Cu-DOTA-polystyrene (4.81 MBq/57.8 μg/100 μL) was orally administered to mice. Then PET was acquired at 1, 6, 12, 24, and 48 h after. PET data were acquired for 15 min within 350–650 keV. The PET data were reconstructed using an SP-MAP (target resolution 3). The voxel size was 0.776 × 0.776 × 0.796 mm^3. Regions of interest (ROI) were drawn in the stomach, liver, and intestine using ASIpro (Siemens Medical Solutions, Germany) after co-registration of CT and PET. SUV_{max} was then calculated.

Bio-distribution (Bio-D) study

The accumulated radioactivity concentration (%ID/g) in each organ were measured at corresponding time after administration of [^{64}Cu]Cu-DOTA-polystyrene or ^{64}Cu.

Ex vivo tissue-radio thin-layer chromatography (Ex vivo-radioTLC)

Ex vivo-radioTLC assays were performed to determine whether the detected gamma rays emitted from the tissues were emitted from ^{64}Cu or [^{64}Cu]Cu-DOTA-polystyrene at each time point. Homogenized samples were lysed in 10% SDS-PBS (pH 7.4) instead of strong acid because low pH (≤ 1) induces de-chelation of ^{64}Cu from DOTA within 1 min (*19*). Similarly, low pH in the stomach can disrupt stable chelation of [^{64}Cu]Cu-DOTA, and this phenomenon was identified from *ex vivo*-radioTLC of the stomach at later time points.

Statistical analysis

The data are presented as the mean with standard deviation. Student's t-test was performed using PRISM (ver. 5.0. GraphPad, San Diego, CA, USA). * denotes $P < 0.05$; ** denotes $P < 0.005$.

RESULTS

Synthesis and Radiolabeling

DOTA-conjugation was confirmed by HPLC and FT-IR spectrometer (Fig. 2A and Supplemental Fig. 1). 184.78±0.26 nmol of DOTA was conjugated per milligram of polystyrene. The particle sizes of polystyrene and DOTA-polystyrene were 223–224 nm, and no aggregation was observed (in either set of results) after the DOTA-conjugation reaction (Fig. 2B and C). Radiochemical yield of [^{64}Cu]Cu-DOTA-polystyrene was 92.07±3.20% and radiochemical purity was 96.39±1.66% (Supplemental Fig. 2A).

In vitro stability study

No significant de-chelation was observed after 48 h in PBS (96.34%), pH 2 (91.68%), human serum (93.23%), or mouse serum (96.83%). The *in vitro* stability study demonstrated that ^{64}Cu-labeled polystyrene was stable for the time period used in this study (Supplemental Fig. 2B).

PET/CT imaging

Fig. 3 and Supplemental Fig. 3 show the representative PET data at 1, 6, 12, 24, and 48 h after oral administration of [^{64}Cu]Cu-DOTA-polystyrene and/or ^{64}Cu. The corresponding time activity curve (TAC) is shown for the stomach, liver, and intestine. PET images demonstrate that [^{64}Cu]Cu-DOTA-polystyrene remained for up to 24 h in the stomach. The SUV_{max} of [^{64}Cu]Cu-DOTA-polystyrene in the stomach was 35.42±4.25 at 1 h, 36.22±3.91 at 6 h, 37.32±1.34 at 12 h, 22.68±4.81 at 24 h, and 0.20±0.03 at 48 h. Polystyrene began its transit to the intestine within 1 h. The SUV_{max} of [^{64}Cu]Cu-DOTA-polystyrene in the intestine was 41.93±22.59 at 1 h, 45.29±19.79 at 6 h, 33.84±7.10 at 12 h, 15.59±3.22 at 24 h, and 0.72±0.75 at 48 h.

The *in vivo* absorption and distribution pattern of ^{64}Cu observed using PET was statistically different at each PET measurement point (Fig. 3, *$p<0.05$, **$p<0.005$).
The SUV_{max} in stomach (marked “S” in Fig. 3) were 35.42±4.25 for [^{64}Cu]Cu-DOTA-polystyrene and 8.39±6.98 for ^{64}Cu at 1 h post administration. The SUV_{max} of [^{64}Cu]Cu-DOTA-polystyrene was 4.22, 4.67, 7.40, and 7.83-fold greater in the stomach (compared to the SUV_{max} of ^{64}Cu) at 1, 6, 12, and 24 h, respectively (*$p<0.05$, **$p<0.005$). Moreover, the area under the

curve (AUC) for [^{64}Cu]Cu-DOTA-polystyrene was 6.03 times greater in the stomach (AUC for [^{64}Cu]Cu-DOTA-polystyrene, 1034.0; AUC for ^{64}Cu, 171.2).

The SUV_{max} in the intestine (marked "I" in Fig. 3) were 45.29±19.75 for [^{64}Cu]Cu-DOTA-polystyrene and 8.40±3.36 for ^{64}Cu at 1 h post administration. The SUV_{max} of [^{64}Cu]Cu-DOTA-polystyrene was 5.38, 23.26, and 19.43-fold greater in the intestine (compared to the SUV_{max} of ^{64}Cu) at 6, 12, and 24 h, respectively (*$p<0.05$, **$p<0.005$). Moreover, the AUC for [^{64}Cu]Cu-DOTA-polystyrene was 4.95 times greater in the intestine (AUC for [^{64}Cu]Cu-DOTA-polystyrene, 933.1; AUC for ^{64}Cu, 188.3).

The SUV_{max} in the liver (marked "L" in Fig. 3) were 0.04±0.03 for [^{64}Cu]Cu-DOTA-polystyrene and 1.83±0.75 for ^{64}Cu at 1 h post administration. The SUV_{max} of [^{64}Cu]Cu-DOTA-polystyrene was 0.02, 0.01, 0.01, and 0.04-fold lower in the liver (compared to that of ^{64}Cu) at 1, 6, 12, and 24 h, respectively (*$p<0.05$, **$p<0.005$). Moreover, the AUC for [^{64}Cu]Cu-DOTA-polystyrene was 0.07 times lower in the liver (AUC for [^{64}Cu]Cu-DOTA-polystyrene, 3.78; AUC for ^{64}Cu, 53.16). A higher uptake of ^{64}Cu in the liver was observed on PET. This was because ^{64}Cu was largely adsorbed by albumin and transcuprein and then carried to the liver (*20*). We also found that both [^{64}Cu]Cu-DOTA-polystyrene and ^{64}Cu were partly excreted in feces (marked "F" in Fig. 3).

Bio-distribution (Bio-D) study

Fig. 4 shows the result of Bio-D in the interesting organs. Overall, the accumulation pattern of Bio-D was similar to that of SUV in the PET images. In the stomach, %ID/g of [^{64}Cu]Cu-DOTA-polystyrene was 2.01, 2.31, 8.28, 3.61, and 13.27-fold greater compared to that of ^{64}Cu at each time point, respectively (*$p<0.05$, **$p<0.005$). In the small intestine, %ID/g of [^{64}Cu]Cu-DOTA-polystyrene was 6.88, 3.44, 2.50, and 11.44-fold greater in the small intestine compared to that of ^{64}Cu, respectively (*$p<0.05$, **$p<0.005$). In the large intestine, %ID/g of [^{64}Cu]Cu-DOTA-polystyrene was 3.98, 2.27, 3.11, and 13.74-fold greater in the stomach compared to that of ^{64}Cu, respectively (*$p<0.05$, **$p<0.005$). In the liver, %ID/g of [^{64}Cu]Cu-DOTA-polystyrene was 0.10, 0.22, 0.18, 0.49, and 0.10-fold lower in the liver compared to that of ^{64}Cu, respectively (*$p<0.05$, **$p<0.005$). Additionally, we observed transit of [^{64}Cu]Cu-DOTA-polystyrene to the liver, spleen, heart, blood, lung, kidney, bladder, and testis.

In contrast, most of the ^{64}Cu accumulated in the large intestine, stomach, and small intestine at 1 h post administration. ^{64}Cu then quickly transitioned to other organs, including the liver. Greater %ID/g accumulation of ^{64}Cu was observed in all other organs, including the liver (9.59-fold), spleen (12.0-fold), heart (7.85-fold), blood (5.83-fold), lung (25.69-fold), kidney (26.92-fold), bladder (1.35-fold), brain (1.36-fold), and testis (6.35-fold) compared to [^{64}Cu]Cu-DOTA-polystyrene.

Ex vivo tissue-radio thin-layer chromatography (Ex vivo-radioTLC)

The *ex vivo*-radioTLC assay results in other tissues (liver, small, and large intestine) demonstrated that the radiation signal was from [^{64}Cu]Cu-DOTA-polystyrene, not ^{64}Cu (Supplemental Fig. 4).

DISCUSSION

We first identified the *in vivo* distribution of MPs in mice. To accomplish this, we labeled MP polystyrene with the radioisotope ^{64}Cu, [^{64}Cu]Cu-DOTA-polystyrene (radiolabeled MP polystyrene) was then orally administered to mice. PET was used to trace the absorption and distribution of [^{64}Cu]Cu-DOTA-polystyrene. Next, *ex vivo* biodistribution studies confirmed [^{64}Cu]Cu-DOTA-polystyrene accumulation in specific organs. *Ex vivo*-radioTLC was used to confirm that the detected gamma rays originated from [^{64}Cu]Cu-DOTA-polystyrene. Exposure to MPs in food and water through oral administration is a significant environmental and health problem (*21*-*23*). However, as discussed earlier, it is extremely likely that MPs are widely distributed within the food we eat.

The advantage of PET is that it is possible to observe the *in vivo* absorption, distribution, metabolism, and excretion of substances labeled with radioactive isotopes without sacrificing the animal (*16*). Although fluorescence is commonly used for *in vivo* exposure and biodistribution studies, fluorescence in animal bodies can be absorbed by bone and soft tissues, and prolonged exposure to ultraviolet light can result in bleaching and loss of fluorescence intensity (*24*). Therefore, quantification of fluorescent images is limited compared to PET imaging. In addition, when using MPs conjugated with fluorescent dyes, animals must be sacrificed to observe the absorption and accumulation of MPs over time. [^{64}Cu]Cu-DOTA-polystyrene transit and absorption were observed within the same animal using PET, without sacrificing the animal.

In this study, we first observed the *in vivo* pathways (absorption, distribution, metabolism, and excretion) of an MP labeled with a radioisotope using PET. In order to trace the polystyrene after oral administration, we selected ^{64}Cu and *p*-SCN-Bn-DOTA for the radiolabeling of plastic particles. We subsequently confirmed that the detected radiation was emitted from the [^{64}Cu]Cu-DOTA-polystyrene, and not from ^{64}Cu, using *ex vivo*-radioTLC. DOTA-NHS ester and *p*-SCN-Bn-DOTA are frequently used chelators (*19*). DOTA conjugation was confirmed by FT-IR spectroscopy, because the functional groups of DOTA show specific bands (Supplemental Fig. 1).

The Bio-D study also demonstrated that the distribution of [^{64}Cu]Cu-DOTA-polystyrene was different from that of ^{64}Cu. The Bio-D study provided quantification of [^{64}Cu]Cu-DOTA-polystyrene accumulation in each organ, even at low levels of emitted gamma ray. Using Bio-D,

we observed the transit and accumulation of [^{64}Cu]Cu-DOTA-polystyrene within the gastrointestinal tract (stomach, intestine, and liver), circulatory organs (heart, lung, and blood), renal system (kidney and bladder), and even in the brain, at 1 h after oral administration.

In contrast, orally administered ^{64}Cu was rapidly removed from the stomach, small intestines, and large intestine, before transit to the other organs, including the liver (Fig. 4). We also observed a higher SUV in the liver on PET for the ^{64}Cu orally administered group (Fig. 3). In a previous report, accumulation of ^{64}Cu in the liver was observed on PET (*20*). For kidney and spleen, the levels of ID/g (1 <%ID/g <10) were 3.47 and 1.08 at 1 h, respectively. For bladder, testis, heart, lung, and blood, the levels of ID/g (%ID/g <1) were 0.70, 0.22, 0.55, 0.92, and 0.21 at 1 h, respectively. The rapid distribution of orally administered ^{64}Cu to the other organs may have occurred because digestive fluid may facilitate solubilization of ^{64}Cu in the stomach. ^{64}Cu was partly cleared in feces after transit through the gastrointestinal tract, and the remaining ^{64}Cu was distributed to other organs, including the liver.

In mice, normal gastric pH is approximately 3.0 (*25*). During transit through the stomach, [^{64}Cu]Cu-DOTA-polystyrene may encounter harsh conditions, possibly de-chelating ^{64}Cu. However, our *ex vivo*-radioTLC assay assured that there was no de-chelation of ^{64}Cu in the stomach and liver at 1 h through comparison data between ^{64}Cu and [^{64}Cu]Cu-DOTA-polystyrene. According to the data, the detected signal from PET and Bio-D at 1 h in all other organs, including the liver, was from [^{64}Cu]Cu-DOTA-polystyrene, not de-chelated ^{64}Cu. Although the acidity of the stomach did affect de-chelation at 6 h post-administration, the other organs were not influenced by de-chelation of ^{64}Cu from radioTLC (shown in Supplemental Fig. 4). Therefore, each data obtained from PET imaging and biodistribution was confirmed with [^{64}Cu]Cu-DOTA-polystyrene. Consequently, the de-chelation of ^{64}Cu could be negligible. (Fig. 4, *p<0.05, **p<0.005).

Recently, several animal studies have been published on the effects of MPs (*26-29*). MP ingestion may induce behavioral disorders in mice (*30*). Therefore, it is important to observe how MPs are distributed in the body following ingestion. Remarkably, Bio-D demonstrated that [^{64}Cu]Cu-DOTA-polystyrene was distributed to all tested organs, including the testis, even after a one-time single dose. Thus, [^{64}Cu]Cu-DOTA-polystyrene may transit and accumulate in all organs even 1 h after oral administration. According to a recent report, a four-week exposure to

polystyrene (1.0 % w/v, 10 mL) induced male reproductive dysfunction in mice (*31*). Based on that mouse study and on our present results, we assumed that at least four weeks of polystyrene exposure may induce hazardous effects on individual organs such as digestive organs, circulatory organs, and excretory organs.

We used BALB/c nude mice because we aimed to assess the tumorigenesis after longitudinal polystyrene exposure for further study. When different strains of mouse were used, possibly different absorption, distribution, metabolism, and elimination of polystyrene might be observed during PET imaging.

The polystyrene used in these experiments have been surface coated with amines, and it seems likely that this may affect their biodistribution. Polystyrene is a highly hydrophobic particle, and the addition of multiple primary amines (hydrophilic and positively charged at physiological pH) and DOTA chelators (hydrophilic and negatively charged at physiological pH) on the surface may influence biodistribution. Hydrophobic compounds and aggregates tend to show uptake and retention in the liver, and therefore uptake in the liver may be influenced by the surface modifications. Even if radiotracers were prepared from same material, several factors, which are size, shape, and surface charge, can affect biodistribution and clearance. Generally, small nanoparticles penetrate capillary walls more easily than large nanoparticles, and positively charged nanoparticles are cleared more quickly by macrophages (*32-34*). Smaller and negatively charged silica nanoparticles have enhanced intestinal permeation by opening tight junctions (*35*). In this study, we selected a sphere-shaped and 0.2 μm-sized polystyrene and observed no significant difference of size and shape after DOTA conjugation. ^{64}Cu-labeled DOTA-polystyrene contains uncoordinated carboxylic acids, which have negative charges, and free amines, which have positive charges at physiological pH. These surface charge may affect the permeability of gastrointestinal tract and distribution. Recent fluorescence conjugated MP studies indicated that biodistribution of MP was dependent on size of the particles (*26*,*36*). According to the result of ref (*26*), 5-μm sized MP was more accumulated in the kidney and gut compared to when use of 20 μm sized MP. Therefore, possibly, the smaller amount of radioisotope labelled MP could be accumulated in the mice organ when larger sized MP was used.

CONCLUSION

Our results demonstrate the utility of PET for visualizing the absorption and distribution of polystyrene microplastics radiolabeled with ^{64}Cu. PET provides information on the accumulation of MPs *in vivo* and can provide information on how each organ could be affected following continuous MP exposure. The biological effects of long-term exposure to MPs in each organ affected in this study will be evaluated in future studies.

ACKNOWLEDGMENTS

Thank you for Dr. Kwang il Kim (first author of ref (*20*)) for helpful discussions regarding the accumulation of ^{64}Cu on PET and Dr. Sairan Eom for kind support of sample preparation for FE-SEM and DLS. This study was funded by the Ministry of Science and ICT (MSIT), Republic of Korea. (NRF-2020R1F1A1061476, 2021M2E8A1039980, 50536-2021, 50461-2021).

KEY POINTS

QUESTION: Microplastic (MP) cause environmental threat and human health risk. Because MP was widely detected in food, we can assume that MPs are ingested along with the contaminated food. To understand the absorption path for MPs ingested with foods we eat, ^{64}Cu-labeled polystyrene was orally administered and then PET imaging and ex vivo biodistribution was obtained.

PERTINENT FINDINGS: The absorption path and distribution of [^{64}Cu]Cu-DOTA-polystyrene were determined using positron emission tomography (PET) over 48 h. PET images demonstrated that [^{64}Cu]Cu-DOTA-polystyrene accumulated in stomach and began to transit to the intestine within 1 h. [^{64}Cu]Cu-DOTA-polystyrene accumulation in the liver was also observed.

IMPLICATIONS FOR PATIENT CARE: Based on accumulation of [^{64}Cu]Cu-DOTA-polystyrene in vivo, we can assume long term exposure of polystyrene may induce the potential risks to human health.

REFERENCES

1. EFSA CONTAM Panel. Presence of microplastics and nanoplastics in food, with particular focus on seafood. *EFSA J*. 2016;14:4501.

2. Ferreira P, Fonte E, Soares ME, Carvalho F, Guilhermino L. Effects of multi-stressors on juveniles of the marine fish Pomatoschistus microps: Gold nanoparticles, microplastics and temperature. *Aquat Toxicol.* 2016;170:89-103.

3. Rochman CM, Hoh E, Kurobe T, Teh SJ. Ingested plastic transfers hazardous chemicals to fish and induces hepatic stress. *Sci Rep.* 2013;3:3263.

4. Lu Y, Zhang Y, Deng Y, et al. Uptake and accumulation of polystyrene microplastics in zebrafish (*Danio rerio*) and toxic effects in liver. *Environ Sci technol.* 2016;50:4054-4060.

5. Von Moos N, Burkhardt-Holm P, Köhler A. Uptake and effects of microplastics on cells and tissue of the blue mussel *Mytilus edulis* L. after an experimental exposure. *Environ Sci technol*. 2012;46:11327-11335.

6. Desforges JP, Galbraith M, Ross PS. Ingestion of Microplastics by Zooplankton in the Northeast Pacific Ocean. *Arch Environ Contam Toxicol.* 2015;69:320-330.

7. Cole M, Lindeque PK, Fileman E, et al. Microplastics alter the properties and sinking rates of zooplankton faecal pellets. *Environ Sci Technol.* 2016;50:3239-3246.

8. Avio CG, Gorbi S, Milan M, et al. Pollutants bioavailability and toxicological risk from microplastics to marine mussels. *Environ Pollut.* 2015;198:211-222.

9. Browne MA, Dissanayake A, Galloway TS, Lowe DM, Thompson RC. Ingested microscopic plastic translocates to the circulatory system of the mussel, *Mytilus edulis* (L.). *Environ Sci Technol.* 2008;42:5026-5031.

10. Chua EM, Shimeta J, Nugegoda D, Morrison PD, Clarke BO. Assimilation of polybrominated diphenyl ethers from microplastics by the marine amphipod, Allorchestes compressa. *Environ Sci Technol.* 2014;48:8127-8134.

11. Green DS. Effects of microplastics on European flat oysters, Ostrea edulis and their associated benthic communities. *Environ Pollut*. 2016;216:95-103.

12. Devriese LI, van der Meulen MD, Maes T, et al. Microplastic contamination in brown shrimp (Crangon crangon, Linnaeus 1758) from coastal waters of the Southern North Sea and Channel area. *Mar Pollut Bull.* 2015;98:179-187.

13. Watts AJ, Lewis C, Goodhead RM, et al. Uptake and retention of microplastics by the shore crab Carcinus maenas. *Environ Sci Technol.* 2014;48:8823-8830.

14. Cole M, Lindeque P, Fileman E, et al. Microplastic ingestion by zooplankton. *Environ Sci Technol.* 2013;47:6646-6655.

15. De Witte B, Devriese L, Bekaert K, et al. Quality assessment of the blue mussel (*Mytilus edulis*): Comparison between commercial and wild types. *Mar Pollut Bull.* 2014;85:146-155.

16. Spinelli T, Calcagnile S, Giuliano C, et al. Netupitant PET imaging and ADME studies in humans. *J Clin Pharmacol.* 2014;54:97-108.

17. Lee CH, Shim HE, Song L, et al. Efficient and stable radiolabeling of polycyclic aromatic hydrocarbon assemblies: in vivo imaging of diesel exhaust particulates in mice. *Chem Commun (Camb).* 2019;55:447-450.

18. Shim HE, Lee JY, Lee CH, et al. Quantification of inhaled aerosol particles composed of toxic household disinfectant using radioanalytical method. *Chemosphere.* 2018;207:649-654.

19. Price TW, Greenman J, Stasiuk GJ. Current advances in ligand design for inorganic positron emission tomography tracers ^{68}Ga, ^{64}Cu, ^{89}Zr and ^{44}Sc. *Dalton Trans.* 2016;45:15702-15724.

20. Kim KI, Jang SJ, Park JH, et al. Detection of increased ^{64}Cu uptake by human copper transporter 1 gene overexpression using PET with $^{64}CuCl_2$ in human breast cancer xenograft model. *J Nucl Med.* 2014;55:1692-1698.

21. Yang Y, Wei C, Liu J, et al. Atorvastatin protects against postoperative neurocognitive disorder via a peroxisome proliferator-activated receptor-gamma signaling pathway in mice. *J Int Med Res.* 2020;48:300060520924251.

22. Cho Y, Shim WJ, Jang M, Han GM, Hong SH. Abundance and characteristics of microplastics in market bivalves from South Korea. *Environ Pollut.* 2019;245:1107-1116.

23. Oliveri Conti G, Ferrante M, Banni M, et al. Micro- and nano-plastics in edible fruit and vegetables. The first diet risks assessment for the general population. *Environ Res.* 2020;187:109677.

24. Robson AL, Dastoor PC, Flynn J, et al. Advantages and limitations of current imaging techniques for characterizing liposome morphology. *Front Pharmacol.* 2018;9:80.

25. McConnell EL, Basit AW, Murdan S. Measurements of rat and mouse gastrointestinal pH, fluid and lymphoid tissue, and implications for in-vivo experiments. *J Pharm Pharmacol.* 2008;60:63-70.

26. Deng Y, Zhang Y, Lemos B, Ren H. Tissue accumulation of microplastics in mice and biomarker responses suggest widespread health risks of exposure. *Sci Rep.* 2017;7:46687.

27. Lu L, Wan Z, Luo T, Fu Z, Jin Y. Polystyrene microplastics induce gut microbiota dysbiosis and hepatic lipid metabolism disorder in mice. *Sci Total Environ.* 2018;631-632:449-458.

28. Stock V, Bohmert L, Lisicki E, et al. Uptake and effects of orally ingested polystyrene microplastic particles in vitro and in vivo. *Arch Toxicol.* 2019;93:1817-1833.

29. Lei L, Wu S, Lu S, et al. Microplastic particles cause intestinal damage and other adverse effects in zebrafish Danio rerio and nematode Caenorhabditis elegans. *Sci Total Environ.* 2018;619-620:1-8.

30. da Costa Araujo AP, Malafaia G. Microplastic ingestion induces behavioral disorders in mice: A preliminary study on the trophic transfer effects via tadpoles and fish. *J Hazard Mater.* 2021;401:123263.

31. Jin H, Ma T, Sha X, et al. Polystyrene microplastics induced male reproductive toxicity in mice. *J Hazard Mater.* 2021;401:123430.

32. Mitchell MJ, Billingsley MM, Haley RM, Wechsler ME, Peppas NA, Langer R. Engineering precision nanoparticles for drug delivery. *Nat Rev Drug Discov.* 2021;20:101-124.

33. Blanco E, Shen H, Ferrari M. Principles of nanoparticle design for overcoming biological barriers to drug delivery. *Nat Biotechnol.* 2015;33:941-951.

34. Kou L, Bhutia YD, Yao Q, He Z, Sun J, Ganapathy V. Transporter-guided delivery of nanoparticles to improve drug permeation across cellular barriers and drug exposure to selective cell types. *Front Pharmacol.* 2018;9:27.

35. Lamson NG, Berger A, Fein KC, Whitehead KA. Anionic nanoparticles enable the oral delivery of proteins by enhancing intestinal permeability. *Nat Biomed Eng.* 2020;4:84-96.

36. Ma J, Zhao J, Zhu Z, Li L, Yu F. Effect of microplastic size on the adsorption behavior and mechanism of triclosan on polyvinyl chloride. *Environ Pollut.* 2019;254:113104.

Figures

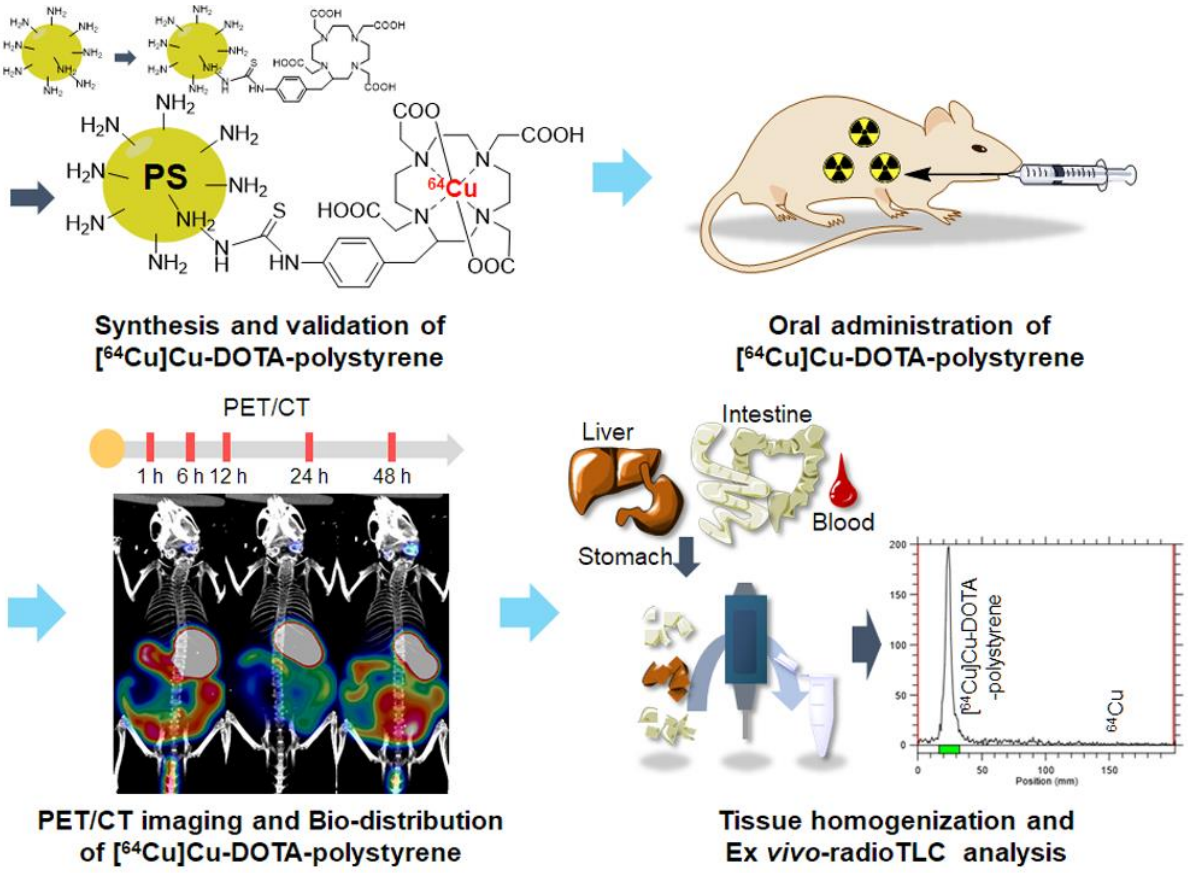

Fig. 1. Schematic of the experiment. [^{64}Cu]Cu-DOTA-polystyrene was synthesized and validated using analytical instruments and radioTLC. [^{64}Cu]Cu-DOTA-polystyrene was orally administrated to mice and PET/CT was performed at 1, 6, 12, 24, and 48 h after the administration of [^{64}Cu]Cu-DOTA-polystyrene. Tissues were weighed and counted at each time point for tissue distribution. An *ex vivo*-radioTLC assay was performed to determine whether the detected gamma rays emitted from the tissue were originated from ^{64}Cu or [^{64}Cu]Cu-DOTA-polystyrene.

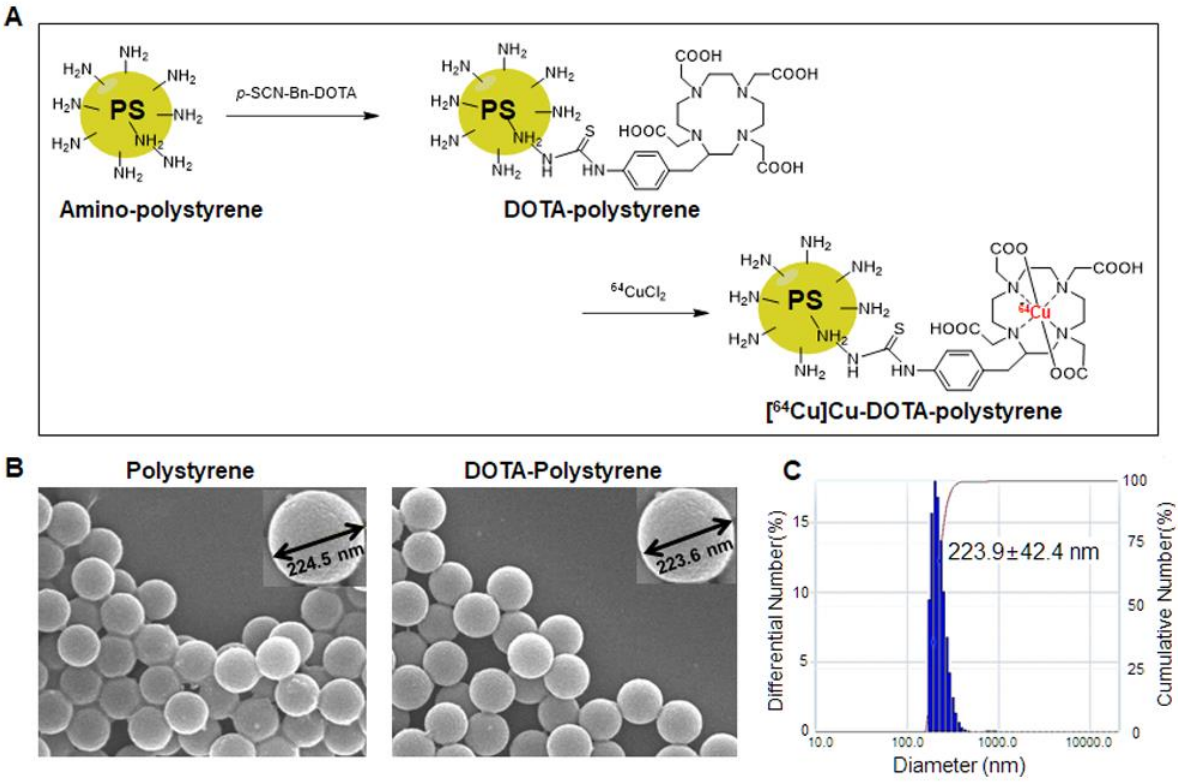

Fig. 2. Synthesis of [^{64}Cu]Cu-DOTA-polystyrene, and physicochemical validation of DOTA-polystyrene using field emission scanning electron microscope (FE-SEM) and dynamic light scattering (DLS). (A) *p*-SCN-Bn-DOTA was conjugated to amine in polystyrene and labeled with ^{64}Cu in pH 5 buffer. (B) The polystyrene particles (left) and DOTA-polystyrene particles (right) show no difference in FE-SEM and DLS. (C) No aggregation of DOTA-polystyrene particles occurred during conjugation.

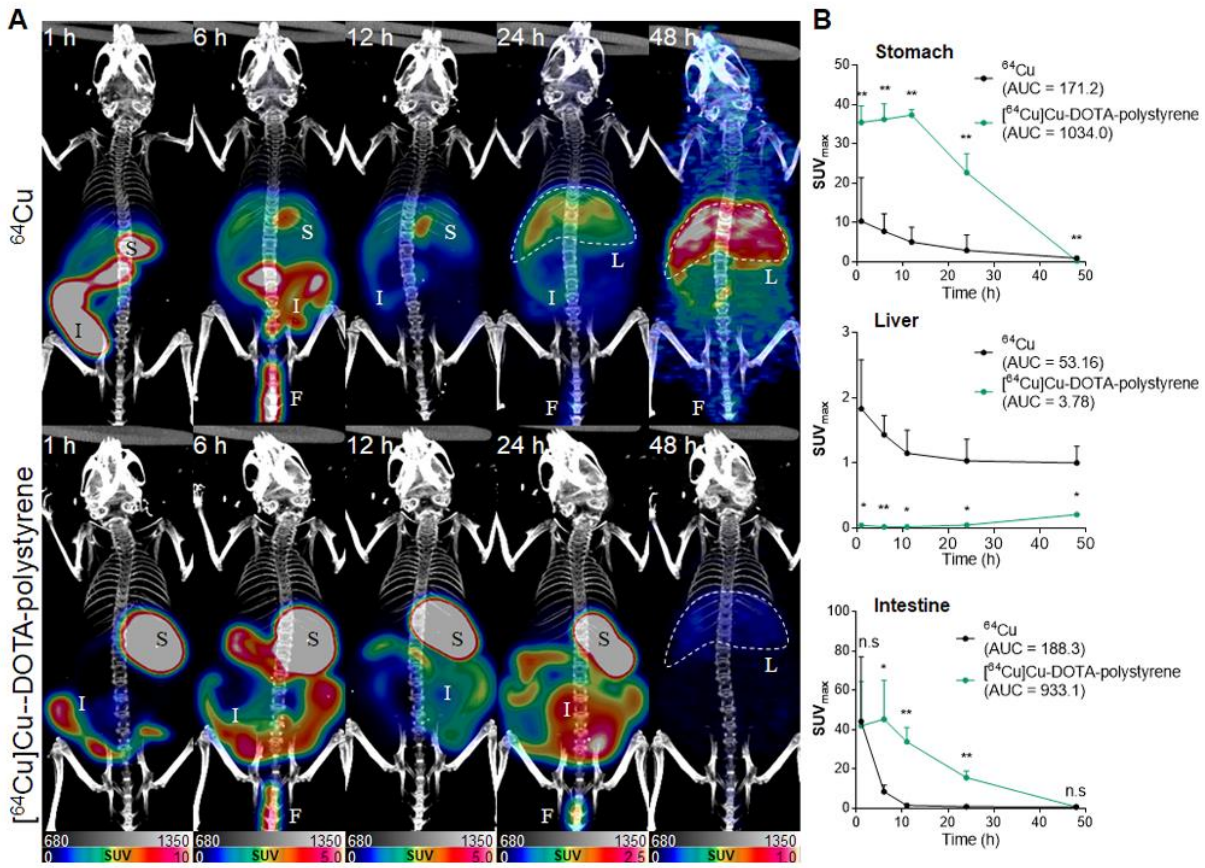

Fig. 3. (A) Representative PET/CT imaging of oral administered [^{64}Cu]Cu-DOTA-polystyrene and/or ^{64}Cu. [^{64}Cu]Cu-DOTA-polystyrene accumulated in the stomach and intestine for 24 h. Uptake of [^{64}Cu]Cu-DOTA-polystyrene was observed in liver at 48 h post administration. However, ^{64}Cu in the stomach and intestinal track was rapidly cleared and transported to the liver. (B) The maximal standard uptake value (SUV_{max}). SUV_{max} of [^{64}Cu]Cu-DOTA-polystyrene was significantly higher than that of ^{64}Cu in the stomach and intestine. In contrast, the SUV_{max} of [^{64}Cu]Cu-DOTA-polystyrene was significantly lower than that of ^{64}Cu in liver. (S, stomach; I, intestine; F, feces; L, liver. n=5, Student's t-test, *$p<0.05$, **$p<0.005$) The image color map reports the SUV value.

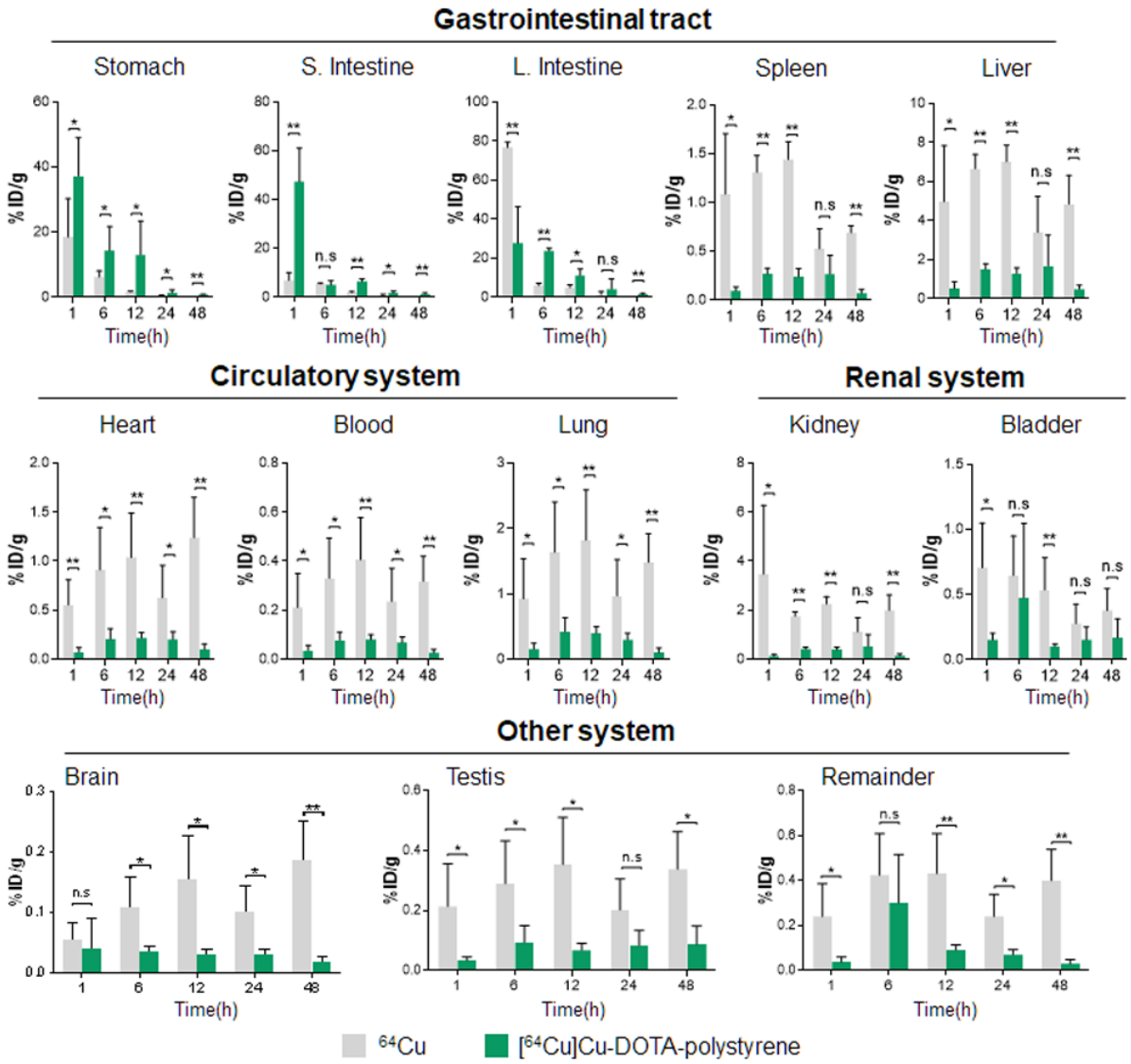

Fig. 4. The bio-distribution results of ^{64}Cu and [^{64}Cu]Cu-DOTA-polystyrene in gastrointestinal tract (stomach, intestine, liver), circulatory organs (heart, lung, blood), renal system (kidney, bladder), and the brain. Overall, the accumulation pattern of Bio-D was similar to that of SUV in PET images. The %ID/g of [^{64}Cu]Cu-DOTA-polystyrene was significantly higher in stomach, small intestines, and large intestine compared to that of ^{64}Cu. However, a lower %ID/g of [^{64}Cu]Cu-DOTA-polystyrene was observed in the liver compared to that of ^{64}Cu. Additionally, we found that [^{64}Cu]Cu-DOTA-polystyrene transited to the gastrointestinal tract (liver, spleen), circulatory system (heart, blood, lung), renal system (kidney, bladder), and even to the brain and testis. In contrast, most of the ^{64}Cu accumulated in the large intestine, stomach, and small

intestine at 1 h post administration. Subsequently, ^{64}Cu transited quickly to other organs, including the liver. Greater %ID/g accumulation of ^{64}Cu was observed in all other organs tested, including the liver, spleen, heart, blood, lung, kidney, bladder, brain, and testis, compared to [^{64}Cu]Cu-DOTA-polystyrene (n=5, student's t-test, *$p<0.05$, **$p<0.005$).

Graphical abstract

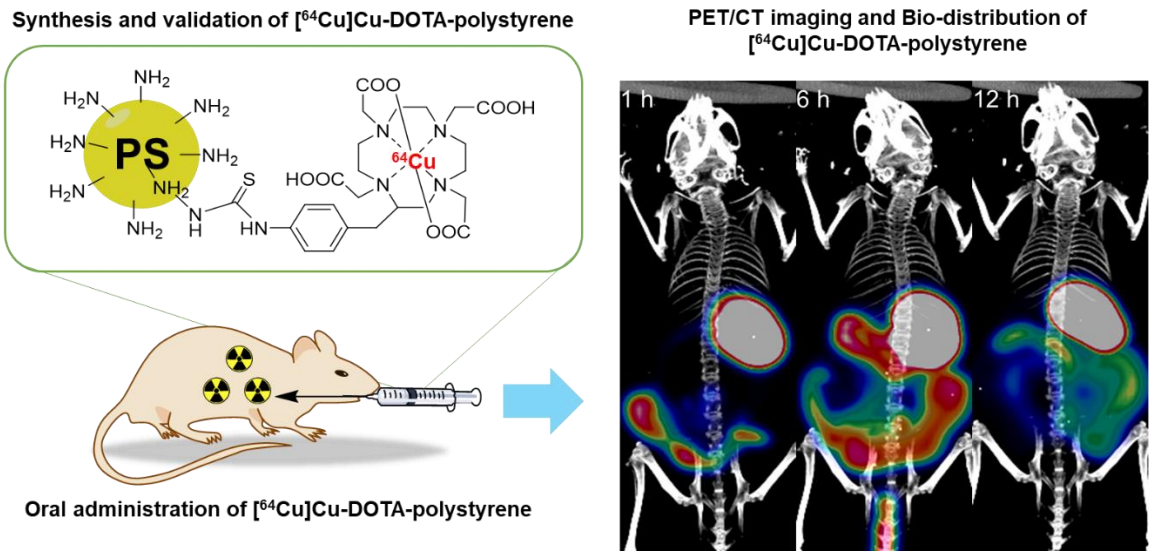

Supplementary Information for
Tracing of Biodistribution of Orally Administered ^{64}Cu-Labeled Polystyrene in Mice

Changkeun Im[1,2,†], Hyeongi Kim[1,†], Javeria Zaheer[1,2], Jung Young Kim[1], Yong-Jin Lee[1], Choong Mo Kang[1,2,*], and Jin Su Kim[1,2,*]

[1]Division of Applied RI, Korea Institute of Radiological and Medical Sciences (KIRAMS), 75 Nowon-ro, Nowon-gu, Seoul 01812, Korea.
[2]Radiological and Medico-Oncological Sciences, University of Science and Technology (UST), 75 Nowon-ro, Nowon-gu, Seoul 01812, Korea.
† These authors contributed equally to this work.
* Choong Mo Kang, Jin Su Kim
Email: ck190@kirams.re.kr, kjs@kirams.re.kr

This PDF file includes:

Supplemental Figure 1 to 4

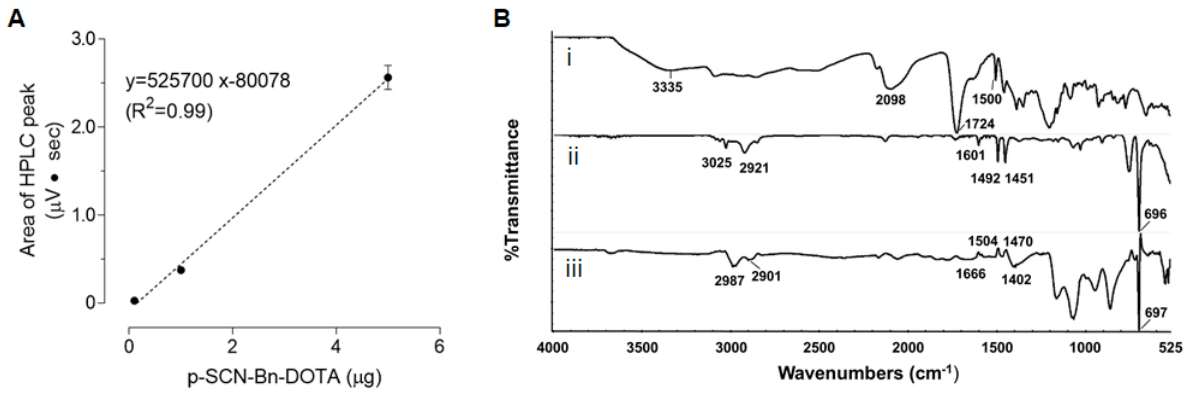

Supplemental Fig. 1. Chemical analysis of DOTA-polystyrene for confirmation of DOTA-conjugation. (A) Standard area curve of three different concentration of *p*-SCN-Bn-DOTA using high performance liquid chromatography (n=3) and moles of DOTA per polystyrene (mg) was determined using a standard curve. (B) Fourier-transform infrared spectrum, (i) *p*-SCN-Bn-DOTA, at 3335 cm^{-1} the presence of amine groups was observed and the isothiocyanate motif vibration was shown at 2098 cm^{-1}. At 1724 cm^{-1} the C=O stretch and at 1500 cm^{-1} the aromatic C-C stretch was identified. The C-H stretch at 1400 cm^{-1} and at C-N were identified (ii) amino-polystyrene, the C-H stretch was assigned at 3000-2800 cm^{-1} and the N-H bend was observed at 1601 cm^{-1} and the C-C stretch was observed at 1600-1400 cm^{-1}. At 720-685 cm^{-1} the aromatic bend was shown. (iii) DOTA-polystyrene, the isothiocyanate region (2098 cm^{-1}) from *p*-SCN-Bn-DOTA was disappeared. At 3000-2800 cm^{-1} the C-H stretch and at 1600-1400 cm^{-1} the C-C stretch were observed. At 720-685 cm^{-1} the aromatic bend was shown.

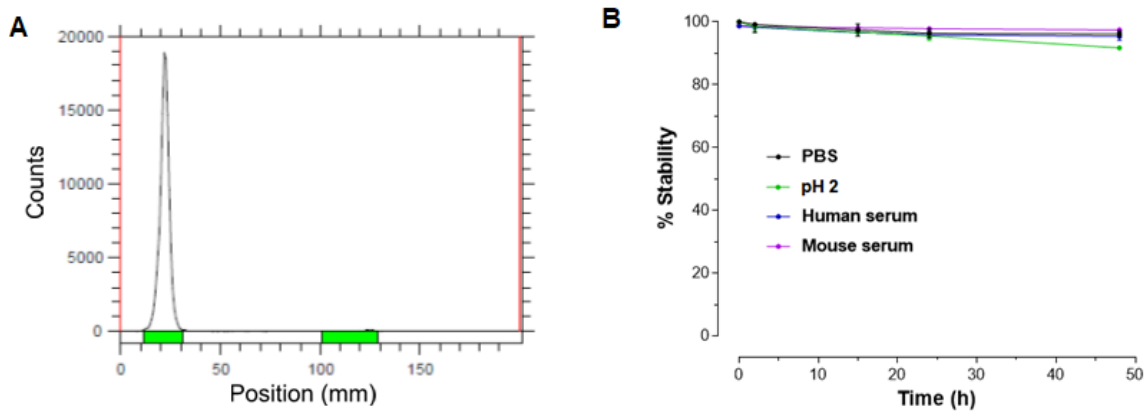

Supplemental Fig. 2. Radiochemical yield and stability of [^{64}Cu]Cu-DOTA-polystyrene. (A) Standard area curve of three different concentration of *p*-SCN-Bn-DOTA using HPLC (n=3) and moles of DOTA per polystyrene (mg) was determined using a standard curve. (B) Radiochemical yield was analyzed using radioTLC developed in 0.1 M citric acid (left peak is [^{64}Cu]Cu-DOTA-polystyrene and right peak is ^{64}Cu). (C) Relative stability results of [^{64}Cu]Cu-DOTA-polystyrene in PBS, pH 2 buffer, human serum, or mouse serum (n=3).

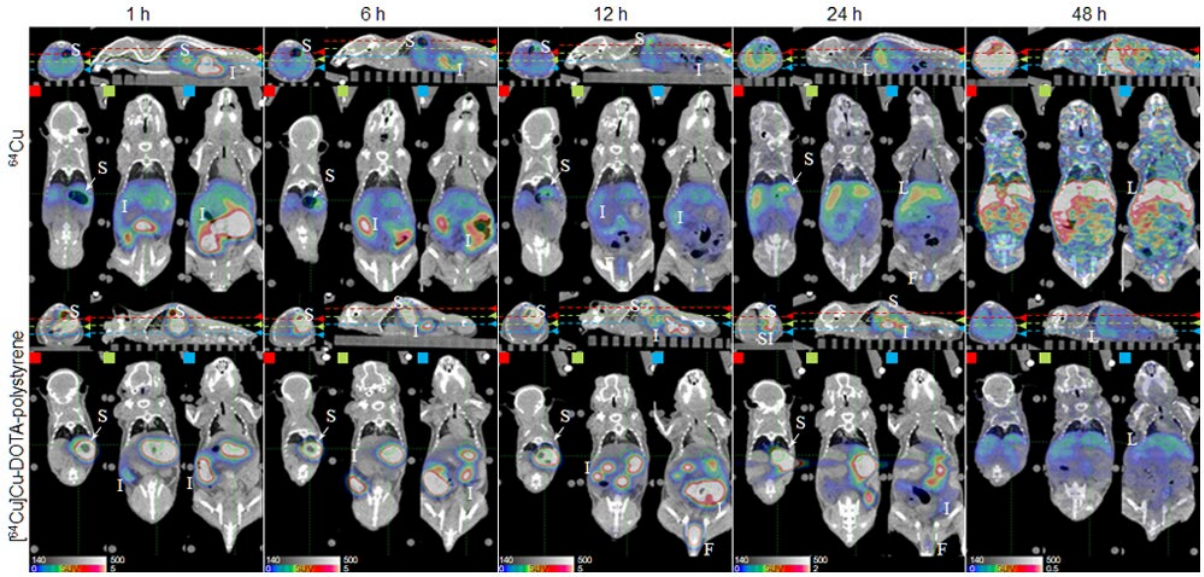

Supplemental Fig. 3. The representative coronal, sagittal, and transverse image of PET/CT at 1, 6, 12, 24, and 48 h post administration of [^{64}Cu]Cu-DOTA-polystyrene or ^{64}Cu. The image color map shows SUV value. Red, green, and blue lines indicate the same slice at different location (S, stomach; I, Intestine; L, liver; F, feces).

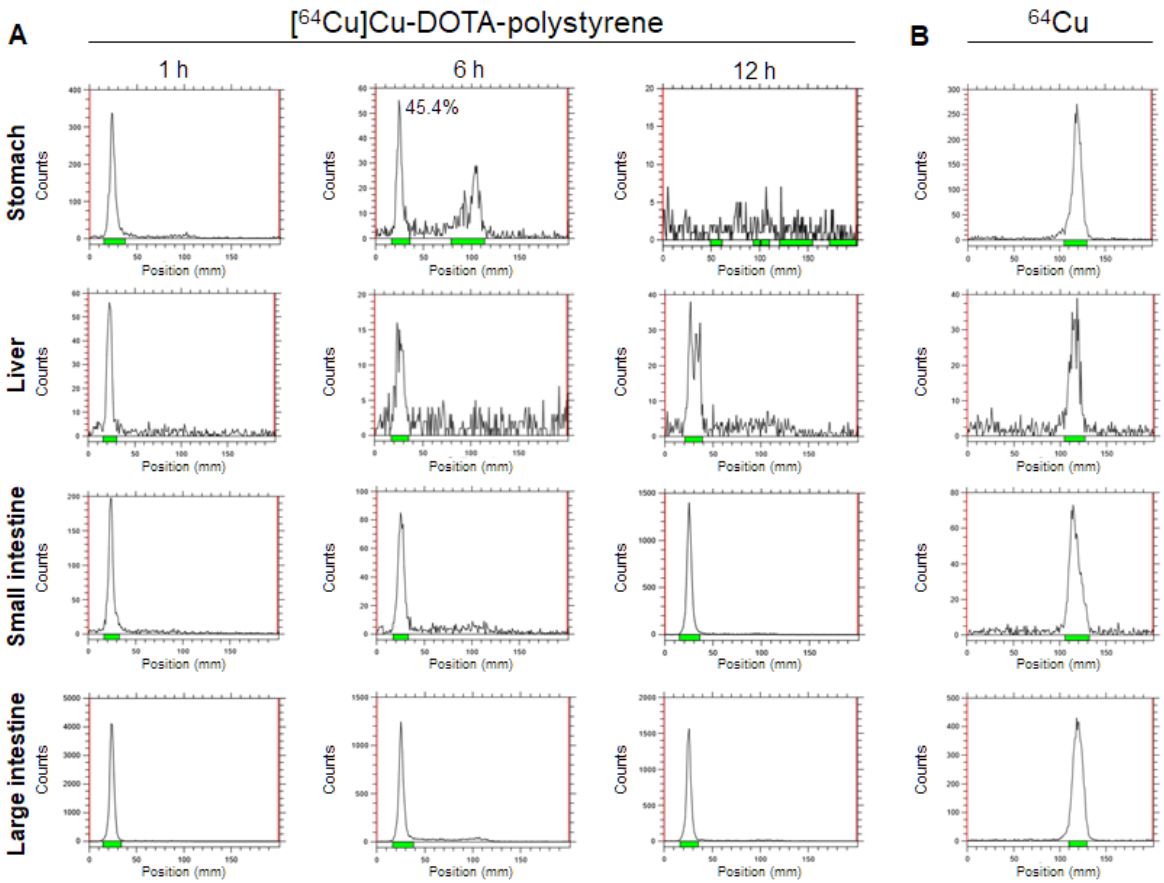

Supplemental Fig. 4. *Ex vivo*-radioTLC analysis of homogenized tissues at 1, 6, and 12 h after oral administration of [^{64}Cu]Cu-DOTA-polystyrene (A) and [^{64}Cu]$CuCl_2$ (B). Instant TLCs were developed in 0.1 M citric acid (left peak is [^{64}Cu]Cu-DOTA-polystyrene and right peak is ^{64}Cu).